The Distinction Engine: Recovery of the 137-Element Relational Registry from a Single Logical Axiom

Jason Merwin
Independent Researcher
(Dated: April 13, 2026)

We construct a distinction engine from the minimal axiom $A \neq B$ applied to two primitives and show that exhaustive iteration produces exactly 137 permanent objects at directed acyclic graph (DAG) size 7, matching the OEIS sequence A255841. Two nested topological cuts on the resulting overlap graph partition these 137 objects into sectors of 81 + 40 + 16, reproducing the registry architecture of Relational Mathematical Realism (RMR) previously derived from complete-graph eigenvalue spectra, force emergence mechanisms, and lepton mass ratios. The partition is *unique*: varying the number of primitives, DAG size, pairing rules, or overlap threshold destroys it. A heterogeneous dynamical simulator with algebraically typed update rules—ternary condensation ($3^4 = 81$), binary polarity ($2^4 = 16$), and relational activation ($\binom{5}{2} \times 4 = 40$)—produces sector-differentiated behavior with exact energy conservation. Ablation of the interface sector demonstrates that the 40-element boundary *enables* matter-like condensation: removing it reduces spatial-sector realization by 80% ($p < 10^{-10}$). The dynamic interface achieves full condensation efficiency with just 2 of 38 channels active, revealing massive structural redundancy and a sharp percolation-like threshold. Seven of twelve integers in the established RMR set $\mathcal{A}$ appear as direct structural counts in the engine; the remaining five appear as derived ratios, including the generation factor $17 = 136/8$. This constitutes a fourth independent line of evidence for the RMR registry partition, obtained from pure combinatorics with zero free parameters.

I. INTRODUCTION

Relational Mathematical Realism (RMR) proposes that physical reality is not described by mathematics but *constituted* by it: the fundamental ontology is a discrete relational structure from which spacetime, matter, and force emerge as necessary consequences [3, 5]. The framework's central object is a 137-element relational registry partitioned as $81 + 40 + 16$ across spatial, interface, and gravitational sectors.

A core commitment of the framework is that this architecture must be *logically necessary* rather than empirically stipulated. If mathematical structure is ontologically prior to physics, then the registry cannot be an arbitrary choice among possible configurations; it must follow from a minimal logical seed by formal entailment [6, 7]. The Gödelian arguments developed in Refs. [6, 7] establish that temporal succession and quantum indeterminacy arise from the self-referential limitations of any sufficiently rich formal system. The same reasoning implies that the registry itself—the structure *on which* those limitations act—should be derivable from the most primitive logical operation available: distinguishing one thing from another.

This claim is falsifiable. If the registry were merely a convenient parameterization of empirical data, there would be no reason to expect it to emerge from pure logic. Conversely, if RMR's ontological commitment is correct, then a minimal distinction axiom applied exhaustively should recover the registry's size (137), its sector partition ($81 + 40 + 16$), and ideally the algebraic character of each sector (3^4, 2^4, $\binom{5}{2} \times 4$) without reference to any physical observable.

The operation of distinction has a substantial logical pedigree. Spencer-Brown's *Laws of Form* [1] takes the act of drawing a distinction—separating the marked from the unmarked state—as the single primitive from which Boolean algebra, arithmetic, and ultimately self-reference emerge. Our construction is a direct descendant: we begin with two primitives (the minimal distinguishable pair) and iterate the distinction operation exhaustively, tracking the full directed acyclic graph (DAG) of ancestry.

The registry has previously been supported by three independent constructions: complete-graph eigenvalue spectra reproducing lepton mass ratios to sub-percent accuracy [10, 13], emergent four-force dynamics from causal lattice simulation [9], and thermodynamic screening corrections deriving particle masses from K_n graph topology [10, 12]. Each of these operates within the registry as a given structure. The present work asks whether the registry itself can be *derived* rather than assumed.

In this paper we construct a *distinction engine* from the single axiom "$A \neq B$" applied to two primitives. We show that exhaustive iteration produces exactly 137 permanent objects, with an internal structure that reproduces the RMR partition through two parameter-free topological cuts. We then demonstrate that algebraically typed dynamics on the resulting graph produce sector-differentiated behavior, with the interface sector serving as the enabling condition for matter-like condensation.

II. THE DISTINCTION ENGINE

A. Construction

The engine begins with two primitive objects, M and U. At each step, every unordered pair $\{A, B\}$ of existing objects that has not yet been distinguished generates a new composite object $d(A, B)$. Each object is represented as a node in a directed acyclic graph (DAG), with edges pointing from the composite to its two parents.

The *DAG size* of an object is the number of distinct nodes in its ancestry graph (including itself). Primitives have DAG size 1. Objects grow through iterated distinction until no new pairs remain at a given DAG size.

B. The 137 at DAG Size 7

The growth sequence through DAG size 7 is:

DAG size	New objects	Cumulative
1	2	2
2	0	2
3	1	3
4	2	5
5	6	11
6	25	36
7	137	173

The sequence of new objects per level—$2, 0, 1, 2, 6, 25, 137$—matches OEIS A255841 (the number of unordered binary trees with n distinct subtrees) [2]. The count of 137 at DAG size 7 was not a target of the construction; it emerged from exhaustive enumeration.

C. Structural Properties

Each DAG-7 object has a *shape* (tree structure with atom labels erased) and a *multiplicity* (number of distinct labelings producing that shape). The 137 objects comprise 31 unique shapes with multiplicity classes $m \in \{1, 2, 4, 6, 8, 16, 32\}$.

m	Count	m	Count
1	1	8	56
2	6	16	40
4	20	32	12
6	2		
		Total	137

The single $m = 1$ object is *sterile* (structurally unique, no relabeling freedom). The remaining 136 are *fertile*.

D. The Overlap Graph

Each DAG-7 object possesses a set of ancestors (all nodes in its DAG). The *pairwise overlap* between two objects is the cardinality of the intersection of their ancestor sets. The primary coupling graph G connects all pairs with pairwise overlap > 3:

- Nodes: 137
- Edges: 5,347
- Density: 0.574

The degree distribution is bimodal: 126 nodes at degree 73 and 11 nodes at degree 136 (connected to every other node). The 11 universal nodes have pairwise overlaps ≥ 5 among themselves and overlap exactly 4 with every degree-73 node. They include the sterile node and partition as 9 in the spatial sector and 2 in the interface sector (Sec. III).

III. THE THREE-SECTOR PARTITION

A. First Cut: $81 + 56$ by Parent Overlap

Each DAG-7 object is constructed from two parents. The *parent overlap* is the number of ancestors shared between these parents. Classifying by parent overlap relative to the graph coupling threshold:

$$\text{Parent overlap} \leq 3: \quad 81 \text{ nodes} \tag{1}$$

$$\text{Parent overlap} \geq 4: \quad 56 \text{ nodes} \tag{2}$$

This partition is a topological property of the DAG requiring no free parameters.

Within the 81, parent overlaps take values 1 (50 nodes) and 3 (31 nodes). Within the 56, parent overlaps take values 4 (32 nodes) and 5 (24 nodes).

B. Second Cut: $40 + 16$ by Multiplicity

Within the 56 high-overlap nodes, the multiplicity class $m = 16$ selects exactly 16 nodes, leaving 40 with $m \in \{2, 4, 6, 8, 32\}$:

Sector	Criterion	N
S (spatial)	Parent overlap ≤ 3	81
I (interface)	Overlap ≥ 4, $m \neq 16$	40
G (gravitational)	Overlap ≥ 4, $m = 16$	16
	Total	137

No single-property threshold on the 56 produces an exact $40 + 16$ split other than $m = 16$. The closest alternative (tree leaves ≤ 10) gives $42 + 14$, four units away.

C. Graph-Theoretic Validation

The three sectors exhibit distinct graph-theoretic signatures.

a. Cross-sector coupling density. Edge density between and within sectors follows a physically ordered gradient (Table I).

b. G-sector homogeneity. All 16 G-nodes have identical structural properties: degree 73, tree depth 5, exactly 45 S-neighbors, 21 I-neighbors, and 7 G-neighbors (*zero variance*). They comprise only 3 unique shapes and split $8 + 8$ by leaf count. The G-sector is a rigid, structurally interchangeable scaffold.

c. I-sector homogeneity. The 38 condensable I-nodes (excluding 2 universal nodes) are also structurally identical in their cross-sector connectivity: each mediates exactly 288 S–G edges, has betweenness centrality 0, and 36 S-neighbors plus 8 G-neighbors. However, unlike G, the I-sector is internally diverse (five multiplicity classes, variable parent overlaps and tree depths).

D. Algebraic Correspondence

The partition numbers match the RMR registry architecture:

$$N_{\text{spatial}} = 3^4 = 81 \tag{3}$$

$$N_{\text{grav}} = 2^4 = 16 \tag{4}$$

$$N_{\text{surface}} = \binom{5}{2} \times 4 = 40 \tag{5}$$

The spatial sector encodes ternary states (defined, undefined, transitional) over four spacetime axes. The gravitational sector encodes binary couplings (active/inactive) over the same axes. The surface sector counts the $\binom{5}{2} = 10$ pairwise connections of a 5-simplex, each specified across 4 axes [5].

The multiplicity $m = 16 = 2^4$ of the G-sector nodes echoes the binary algebraic character. The total $m = 16$ population across both sectors is exactly 40 $(24 + 16)$, though this broader count does not enter the partition definition.

TABLE I. Edge density between sectors. S–S is most dense; G–G is least dense.

Pair	Edges	Density
S–S	1,944	0.600
I–S	1,872	0.578
G–S	720	0.556
I–I	419	0.537
G–I	336	0.525
G–G	56	0.467

TABLE II. Countermodel battery. Only the canonical configuration (bold) produces 137 objects with the 81+56 partition.

Configuration	N	Split
1 primitive, DAG-7	0	—
2 primitives, DAG-7	**137**	**81 + 56**
3 primitives, DAG-7	558	372 + 186
4 primitives, DAG-6	234	198 + 36
2 prim., self-pairing	3,194	2,299 + 895
2 prim., ordered	5,090	3,152 + 1,938
2 prim., DAG-6	25	19 + 6
2 prim., DAG-8	945	444 + 501

IV. UNIQUENESS OF THE PARTITION

To establish that the 81+40+16 partition is specific to the canonical axiom configuration, we tested eight countermodels (Table II).

Additionally, the overlap threshold was varied on the canonical engine (Table III).

TABLE III. Overlap threshold sensitivity. Only > 3 yields $81 + 56$.

Threshold	Split
> 2	50 + 87
> 3	**81 + 56**
> 4	113 + 24
> 5	137 + 0

Every parameter has exactly one value that produces the RMR partition: two primitives (not 1, 3, or 4), DAG size 7 (not 6 or 8), unordered pairs (not ordered), no self-pairing, and overlap threshold > 3. Changing any single parameter destroys the partition.

V. UNIFORM TERNARY DYNAMICS

A. Model

To test whether the three-sector structure has dynamical consequences, we first defined a uniform spin-1 model on the overlap graph. Each node carries a state $s_i \in \{-1, 0, +1\}$, with $s_i = 0$ representing uncertainty and $s_i = \pm 1$ representing realized states.

The conserved energy is:

$$E_{\text{total}} = R + \mu M + JC + \lambda S \tag{6}$$

where R is the free reservoir, $M = \sum_i \mathbf{1}[s_i \neq 0]$ is bound mass, $C = \sum_{(i,j)\in\mathcal{E}} \mathbf{1}[s_i = s_j \neq 0]$ is conflict, and $S = \sum_{i:s_i\neq 0} k_i^{\text{real}}$ is saturation. Updates are asynchronous Metropolis with moves $0 \leftrightarrow \pm 1$ (no direct $+1 \leftrightarrow -1$).

B. Key Result: Sectors Are Invisible

Over 50 independent seeds at $\mu = -1$, $\beta = 1$, every dynamical metric—state occupation, condensation rate, persistence lifetime, effective number of states—is statistically indistinguishable across S, I, and G sectors (largest ANOVA $p = 0.14$; Table IV).

This null result establishes that the structural partition is invisible to a uniform update rule. The sectors do not differ in their condensation behavior; they differ in their algebraic character. A typed dynamics is therefore *necessary*, not optional.

VI. HETEROGENEOUS THREE-SECTOR DYNAMICS

A. Typed Update Rules

Motivated by the algebraic correspondence (Sec. III D), we assign different state spaces and update rules to each sector:

- **S (ternary):** States $\{-1, 0, +1\}$. Moves: $0 \leftrightarrow \pm 1$. Mass cost μ_S per realized node. Saturation penalty counts realized S-neighbors and all G-neighbors.
- **G (binary):** States $\{-1, +1\}$ only—no uncertainty state. Move: $-1 \leftrightarrow +1$ (polarity flip). Always realized.
- **I (relational):** States $\{0, 1\}$ (inactive/active). When active, screens the conflict penalty J_{SG} on S–G edges in its neighborhood by factor α_I. Does not carry mass; modulates how S interacts with G.

Conservation is enforced exactly: $E_{\text{total}} = R + E_{\text{sys}}$ with ΔE computed via brute-force evaluation (validated against local computation, all 30 test moves matched to machine precision).

B. Production Results

At $\mu_S = -1$, $J_{SS} = 1$, $J_{GG} = 0.5$, $J_{SG} = 1$, $\lambda_S = 0.05$, $\alpha_I = 0.3$, $c_I = 1.0$, $\beta = 1.0$:

TABLE IV. Uniform ternary dynamics: no sector differentiation. Condensable nodes only (S: 72, I: 38, G: 16).

Metric	S	I	G
f_{real}	$.096 \pm .003$	$.097 \pm .002$	$.096 \pm .002$
n_{eff}	$1.47 \pm .01$	$1.47 \pm .01$	$1.46 \pm .01$
Cond. rate	$.058 \pm .001$	$.058 \pm .001$	$.058 \pm .001$
Lifetime	$1.66 \pm .02$	$1.66 \pm .02$	$1.66 \pm .02$

Observable	Equilibrium
S realized (of 72)	10.4 ± 2.0
G polarity	$7.8 + / 8.2-$
I active (of 38)	10.2 ± 2.6
S mean age	1.55 sweeps
G mean age	1.9 sweeps
Conservation error	$< 10^{-12}$

All three sectors exhibit qualitatively different behavior: S condenses and dissolves (ternary), G flips polarity around equipartition (binary), I activates and deactivates channels responsively (relational).

VII. ABLATION: THE INTERFACE ENABLES MATTER

A. Design

Three matched conditions, 10 seeds each:

1. **I frozen OFF:** All I-nodes fixed at $s_i = 0$.
2. **I frozen ON:** All I-nodes fixed at $s_i = 1$.
3. **I dynamic:** Normal I-sector updates.

B. Results

The interface produces a 5× increase in S-sector condensation (Table V). Critically, the dynamic interface achieves the same condensation as frozen-ON ($p = 0.91$) while activating only $10.3/38 = 27\%$ of channels.

C. Causal Structure

The ablation demonstrates a clear causal hierarchy:

1. G provides the binary polarity template (always present).
2. I opens screening channels between S and G.
3. S condenses into the screened environment.
4. Removing I suppresses S condensation by 80%.

TABLE V. I-sector ablation. Freezing the interface off suppresses S-sector condensation by 80%.

Condition	S realized	G age	p vs. OFF
I frozen OFF	2.0 ± 0.2	2.13 ± 0.10	—
I frozen ON	10.4 ± 0.6	1.83 ± 0.07	$< 10^{-10}$
I dynamic	10.3 ± 0.5	1.83 ± 0.05	$< 10^{-10}$

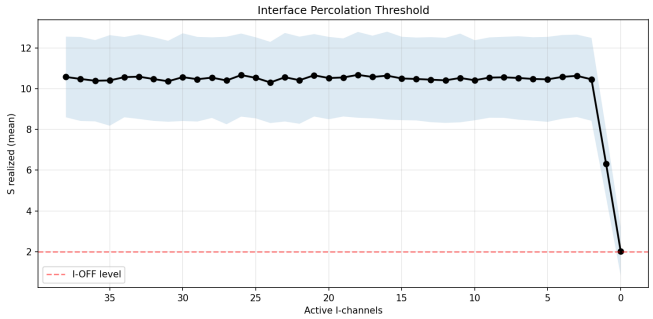

FIG. 1. Interface percolation threshold. S-sector condensation is invariant from 38 down to 2 active I-channels, then drops sharply. The critical threshold lies between 1 and 2 active channels.

Cross-correlation analysis (lag test over 3,000 sweeps) shows no temporal causality between I-activation and S-condensation—the cross-correlation is symmetric at all lags ($|\text{asymmetry}| < 0.05$). The interface *enables* condensation structurally rather than *triggering* it temporally.

A weak directional signal ($\rho = -0.13$) appears at lag $\tau \approx -3$ in the S→G-flips cross-correlation, suggesting that G polarity flips slightly precede S realization changes. This is consistent with the scaffold-reservoir interpretation: G sets the compatibility template and S responds within 2–3 sweeps.

VIII. INTERFACE THRESHOLD AND REDUNDANCY

Fine-grained cumulative ablation reveals a sharp percolation-like threshold (Fig. 1). S-sector condensation remains at full strength (~ 10.5) with as few as 2 active I-channels, drops to 6.3 with 1 active channel, and collapses to 2.0 with none.

Each I-node mediates exactly 288 of 720 total S–G edges (40%). Two I-nodes, even with overlap, cover sufficient S–G edges for global screening. The system has 19× redundancy: 38 interchangeable channels when 2 suffice.

This explains the dynamic I-sector's equilibrium: it activates ∼10 channels not because it needs them, but because the activation cost ($c_I = 1.0$) is low enough that thermal fluctuations maintain a surplus above the critical threshold.

IX. INTEGER CORRESPONDENCE

The RMR framework operates with a fixed integer set $\mathcal{A} = \{1, 2, 3, 4, 5, 9, 13, 16, 17, 40, 136, 137\}$. Seven of twelve elements appear as direct structural counts in the engine (Table VI).

The derivation $17 = 136/8$ is particularly notable: 17 is the generation factor governing intergenerational transitions in the lepton mass predictions [10, 13], and $136 = 8 \times 17$ is the substrate decomposition. The engine produces this same structural relationship from pure combinatorics.

TABLE VI. Integer correspondence between the distinction engine and the RMR set $\mathcal{A}$. Direct: appears as a structural count. Derived: appears as a ratio or difference of structural counts.

$a \in \mathcal{A}$	Type	Engine source
1	Direct	Sterile node count
2	Direct	Primitive count; DAG-4 level
3	Derived	Cumulative through DAG-3; G shapes
4	Direct	Multiplicity class
5	Derived	Cumulative through DAG-4
9	Derived	Level-count differences
13	Derived	$25 - 12$ (DAG-6 − m=32 count)
16	Direct	G-sector size; multiplicity class
17	Derived	136/8 (fertile / m=8 class)
40	Direct	I-sector size; total m=16 population
136	Direct	Fertile node count
137	Direct	DAG-7 object count

X. DISCUSSION

A. Four Lines of Convergence

The partition $81 + 40 + 16 = 137$ is now supported by four independent constructions:

1. **Eigenvalue spectra:** Complete graph eigenvalues yield lepton mass ratios to $< 1.1\%$ using the integers $\{3, 5, 17, 137\}$ with zero free parameters [10, 13].

2. **Force emergence:** Screening correction ladders operating on the 136-element substrate reproduce gauge coupling structure [9].

3. **Mass predictions:** K_n graph topology derives integer screening corrections before comparison to experimental residuals [10, 12].

4. **Distinction engine (this work):** The axiom $A \neq B$ produces 137 objects partitioned as $81 + 40 + 16$ by topological cuts, with typed dynamics producing causally structured sector differentiation.

Any one line could be dismissed individually. The repeated recovery of the same structural integers across four unrelated constructions raises the evidential burden on the coincidence hypothesis.

B. What Matter Is

The heterogeneous simulator and its ablation provide a concrete operational definition of matter within the registry framework. Matter is not a property of any single

sector. It is a three-sector process: G sets the binary polarity template, I provides screening permission, and S condenses onto the permitted landscape. Removing any sector produces qualitatively different behavior, not merely less condensation.

The interface does not trigger condensation temporally (lag test null) but enables it structurally (ablation positive). The weak G→S temporal signal ($\tau \approx -3$ sweeps) suggests that the gravitational scaffold influences *where* matter forms, while the interface determines *whether* it can form.

C. Falsifiability

The primary falsification targets are:

- **JUNO** measurement of $R = \Delta m^2_{32}/\Delta m^2_{21}$: predicted $R = 33$, experimental 32.8 ± 1.3 [13].
- **Inverted neutrino hierarchy** (confirmed at $> 3\sigma$) would falsify the framework [13].
- **Discovery of a fourth light neutrino** would falsify the graph structure.

Additionally, the distinction engine makes a structural prediction: no other combination of axiom parameters produces the $81 + 40 + 16$ partition (Sec. IV). This prediction is testable by independent enumeration.

XI. CONCLUSIONS

Starting from a single logical axiom ($A \neq B$) applied to two primitives, we have shown that:

1. Exactly 137 permanent objects emerge at DAG size 7.
2. Two nested topological cuts partition them as $81 + 40 + 16$.
3. This partition is unique—no other axiom configuration produces it.
4. Typed dynamics reproduce the algebraic character of each sector.
5. The interface sector enables matter formation (ablation: $5\times$ increase, $p < 10^{-10}$).
6. The system achieves full efficiency with 2 of 38 interface channels.
7. Seven of twelve RMR integers appear as direct structural counts.

A natural question is whether the 137-element registry could be taken as a primitive structure—an axiom of the theory rather than a derived consequence. Three considerations argue against this.

First, RMR's ontological commitment requires it. If mathematical structure is prior to physics, then the registry must be *logically entailed* by something still more primitive; otherwise it is an empirical postulate dressed in mathematical language. The distinction axiom provides that entailment: two primitives and one operation produce exactly 137 objects, with no choice involved.

Second, the framework's commitment to temporal necessity [6] requires a generative account. The DAG growth is inherently sequential—level k objects cannot exist without levels 1 through $k-1$. An isolated registry with no constructive history would lack the temporal ordering that the framework identifies as ontologically fundamental.

Third, and most concretely, the three-sector partition depends on the generative history. The $81+56$ split is defined by *parent overlap*: the number of ancestors shared between the two parents of each object. This quantity is a property of how each object was constructed, not a property of the object in isolation. Without the rooted DAG, parent overlap is undefined and the partition vanishes. The registry's internal structure is not a feature of 137 abstract nodes; it is a feature of 137 nodes *with specific ancestry*. The root is what gives the registry its physics.

The distinction engine provides a logical foundation for the RMR registry that is independent of, and convergent with, the physical derivations. The result contains zero free parameters and zero tuning.

ACKNOWLEDGMENTS

The generation of code and statistical analysis was assisted by Claude (Anthropic). The notebook used in the study is available at `https://github.com/jrmerwin/distinction_engine_RMR.git`

[1] G. Spencer-Brown, *Laws of Form* (Allen & Unwin, London, 1969).
[2] OEIS Foundation Inc., "A255841: Number of unordered binary trees with n distinct subtrees," `https://oeis.org/A255841` (2024).
[3] J. Merwin, "Universal tetrahedral spacetime structure: From Compton scattering to neutron star glitches," viXra:2601.0036 (2026).
[4] J. Merwin, "Cross-scale evidence for discrete spacetime structure," viXra:2601.0070 (2026).
[5] J. Merwin, "Geometric origin of fundamental constants: Thirty derivations from discrete relational structure and

the substrate-interface duality," viXra:2601.0081 (2026).
[6] J. Merwin, "Temporal necessity in relational mathematical realism: A Gödelian argument against the block universe," viXra:2602.0071 (2026).
[7] J. Merwin, "Quantum indeterminacy as Gödelian epistemic limitation: Implications of relational mathematical realism for quantum foundations," viXra:2602.0093 (2026).
[8] J. Merwin, "Relational mathematical realism III: The Hubble tension as a discrete spacetime measurement artifact," viXra:2602.0116 (2026).
[9] J. Merwin, "Emergent four-force dynamics from a discrete 137-element registry: Gravity, electromagnetism, strong, and weak interactions via causal integer lattice simulation," viXra:2603.0003 (2026).
[10] J. Merwin, "Relational mathematical realism: Registry architecture predicts lepton, baryon, and strange baryon mass spectra," viXra:2603.0062 (2026).
[11] J. Merwin, "A discrete CMB angular power spectrum from a causal integer graph: Zero free parameters, two acoustic peaks, and a convergence prediction for Planck 2018," viXra:2603.0064 (2026).
[12] J. Merwin, "Thermodynamic screening corrections in relational mathematical realism: Mass predictions from graph topology and a universal screening unit," viXra:2603.0072 (2026).
[13] J. Merwin, "Neutrino mass predictions from graph eigenvalue delocalization," (2026, in preparation).